

Article

An Effective Mercury Ion Adsorbent Based on a Mixed-Matrix Polyvinylidene Fluoride Membrane with Excellent Hydrophilicity and High Mechanical Strength

Ling Cao¹, Xia Wu¹, Fajun He², Xianfeng Meng¹, Wei He¹, Jing Li¹, Guidan Zhu¹, Hehua Zeng^{1,*} and Chuanyi Wang^{3,*} 

¹ School of Chemistry and Chemical Engineering, Changji University, Changji 831100, China; caolinggirl@126.com (L.C.); 13579968602@163.com (X.W.); myn0546@163.com (X.M.); misstimeli@163.com (W.H.); flowerlijing@cj.cn (J.L.); zhuguidan2011@126.com (G.Z.)

² Changji State High-Tech Industrial Development Zone, Changji 831100, China; 18690975921@163.com

³ School of Environmental Science and Engineering, Shaanxi University of Science and Technology, Xi'an 710021, China

* Correspondence: rainy_lily2007@163.com (H.Z.); cywang@ms.xjb.ac.cn (C.W.); Tel.: +86-132-9913-1206 (C.W.)

Abstract: Improving the hydrophilicity and mechanical strength of membranes in water treatment applications remains challenging. In this study, modified vermiculite (VT-M) and a hydrophilic polyvinylpyrrolidone (PVP) were introduced into a polyethyleneimine-functionalized polyvinylidene fluoride composite membrane (PVDF/PEI) to prepare a comprehensively modified mixed-matrix PVDF composite membrane adsorbent that exhibited high mechanical strength and excellent hydrophilicity. The modified composite membrane featured good tensile properties, with a maximum tensile strength of 2.093 MPa, which was 2.5 times that of the PVDF/PEI membrane. After 7 s, the water contact angle of the composite membrane decreased to 0°, leading to significantly improved hydrophilicity. The modified composite membrane exhibited excellent adsorption selectivity for mercury ions, with a fitted maximum adsorption capacity of 807 mg/g. In a mixed-metal ion solution, the selectivity of the membrane for Hg(II) ions was 1.2×10^5 times that for Cd(II) ions. The adsorption mechanism of Hg(II) ions involved chelation, electrostatic attraction, and crystal growth processes. The present work suggests the great potential of mixed-matrix PVDF composite materials in the remediation of mercury-polluted water environments.

Keywords: mixed-matrix membrane; polyvinylidene fluoride; hydrophilicity; mechanical strength; mercury removal



Citation: Cao, L.; Wu, X.; He, F.; Meng, X.; He, W.; Li, J.; Zhu, G.; Zeng, H.; Wang, C. An Effective Mercury Ion Adsorbent Based on a Mixed-Matrix Polyvinylidene Fluoride Membrane with Excellent Hydrophilicity and High Mechanical Strength. *Processes* **2024**, *12*, 30. <https://doi.org/10.3390/pr12010030>

Academic Editors: Blaž Likozar and Suresh K. Bhatia

Received: 31 October 2023
Revised: 11 December 2023
Accepted: 15 December 2023
Published: 22 December 2023



Copyright: © 2023 by the authors. Licensee MDPI, Basel, Switzerland. This article is an open access article distributed under the terms and conditions of the Creative Commons Attribution (CC BY) license (<https://creativecommons.org/licenses/by/4.0/>).

1. Introduction

Mercury (Hg) is an environmental pollutant that has existed in the atmosphere for a long time and has global migration, and the toxicity of mercury has been known by humans for centuries. The main sources of mercury pollution are coal burning, non-ferrous metals, chlor-alkali production, and polyvinyl chloride manufacturing [1–3]. Reducing emission concentrations is the most effective means to control mercury pollution [4–8]. Membrane adsorption has emerged as a promising water treatment method in the field of environmental engineering owing to its easy recovery, simple operation, convenient post-treatment, and potential for repeated use compared to traditional powder adsorption methods [9–13].

Polyvinylidene fluoride (PVDF) is a homopolymer of vinylidene fluoride or a copolymer of vinylidene fluoride with a small number of other fluorinated vinylidene monomers. In addition to its piezoelectric, dielectric, and thermoelectric properties [14,15], PVDF also has good chemical corrosion resistance, high temperature resistance, oxidation resistance, radiation resistance, and other properties, which makes it suitable for membrane fabrication through the phase inversion method [16–20]. Owing to its hydrophobic properties,

PVDF is susceptible to fouling when exposed to water contaminated with hydrophobic organic substances such as organics, proteins, and microorganisms [21–24]. Notably, the mechanical strength of the PVDF membranes is often reduced after functionalization and modification. For example, a strong alkali can induce an elimination reaction in PVDF to remove hydrogen chloride, leading to changes in the molecular structure of PVDF and, consequently, a decrease in the mechanical strength of the membrane [25–28]. In addition, a conventional PVDF membrane lacks active functional groups, limiting its application in heavy metal adsorption. Therefore, improving the comprehensive properties of PVDF membranes is vital for their practical application and is usually achieved through the combination of the advantages of various materials.

Polyethyleneimine (PEI) is one of the most popular adsorbents in recent years. Due to the large number of primary ammonia, secondary amine, and tertiary amine groups, PEI has a high adsorption capacity and selectivity for metal ions. In addition, the amino group has good reactivity and can be easily modified by functional modifications, which broadens the application range of PEI. As an adsorbent, however, PEI has the disadvantages of difficult operation, difficult separation and recovery, and easy loss because it exists in a free molecular state form in the water phase. The shape and material that are more suitable for environmental pollution control can be prepared by supporting PEI on the substrate material through graft or crosslinking modifications. A PVDF/PEI polymer composite membrane prepared in a previous study exhibited good heavy metal adsorption performance but featured poor hydrophilicity [29]. Therefore, the PVDF/PEI membrane was more susceptible to pollution by organic matter, proteins, microorganisms, etc., and was limited in the application of water treatment. As a result, the hydrophilic modification of PVDF/PEI membranes is of great significance.

Polyvinylpyrrolidone (PVP) is a water-soluble linear polyamide with a strong hydrophilic property and is widely used as an additive or modifier in the preparation of hydrophilic materials [30–33]. Despite the high solubility of PVP in water, materials modified by PVP often exhibit unstable hydrophilicity. This instability can be addressed through the addition of crosslinking agents to effectively prevent the loss of PVP during usage and ensure persistent hydrophilic properties. In the present study, to further improve the tensile strength and mechanical properties of the composite membrane, a certain amount of vermiculite (VT) was added to prepare a mixed-matrix PVDF composite membrane co-modified with VT and PVP. A semi-interpenetrating network structure was formed through a crosslinking reaction, and PVP and VT were firmly fixed in the PVDF/PEI matrix. The hydrophilicity, pure water flux, and tensile resistance of the membrane were characterized by the contact angle, water flux, and a tension test, respectively. Through simulation experiments, the adsorption kinetics and equilibrium isotherm were examined systematically to investigate the adsorption mechanism and influencing factors for mercury ions.

2. Materials and Methods

2.1. Materials and Characterizations

Vermiculite with an average size of 8 mm was provided by Xinjiang Nonmetallic Minerals Xiazijie vermiculite Co., Ltd. (Korla, China) 3-aminopropyl triethoxysilane (APTES) was purchased from Sigma-Aldrich (Shanghai, China). PVDF powder was provided from Arkema (Shanghai, China). Details on the other reagents, instrumentation, and analytical methods related to this study are provided in the Supporting Information. The reagents used in all experiments were of analytical grade, and ultrapure water (18.2 M Ω ·cm) was used in all experiments.

2.2. Fabrication of Mixed-Matrix PVDF Adsorption Membrane

The mixed-matrix adsorbent was fabricated via a non-solvent-induced phase inversion method [13]. First, APTES-modified vermiculite (VT-M) was prepared according to the procedure reported in the literature [34]. Then, 2.0 g acidified vermiculite, 1.0 mL water, and 2.0 mL APTES were added to 50 mL ethanol with ultrasonic dispersion for 30 min.

The mixture was then agitated overnight on a magnetic stirrer at 45 °C. The solid was centrifuged and washed repeatedly with ethanol and water to remove excess modifiers and possible hydrolysates. The obtained sample was freeze-dried and named VT-M. Subsequently, 20 mg of VT-M was dispersed in 22 mL of dimethylformamide through sonication. Afterward, 2.7 g of PEI (50%) was fully dissolved in the above suspension at 70 °C, and the mixture was magnetically stirred. Then, 2.0 g of PVDF was added to the mixture. After vigorous agitation for 1 h, 100 mg of PVP was added to the mixed solution. Following 30 min of stirring, 350 µL of epichlorohydrin (ECH) was added dropwise, and the mixture underwent a crosslinking reaction at 70 °C for 8 h to form a brown, viscous solution.

Furthermore, the as-prepared hot-casting solution was uniformly coated on a clean glass plate using a 200 µm air-gap-thick coating rod. The coated glass plate was kept at a constant temperature and humidity (30 °C, RH: 55%) for 30 s, followed by immersion in an ultrapure water bath at room temperature. After 2 h, the nascent membrane was removed from the glass plate and placed in a freshwater bath. The water was then replaced every 4 h to remove any residual solvent. Finally, the membrane was freeze-dried. The pristine PVDF/PEI membrane was prepared using the same procedure, except without the addition of VT-M and PVP.

2.3. Adsorption Tests of Hg(II) Removal

Adsorption and desorption processes were conducted according to the guidelines outlined in reference [29]. All details are provided in the Supporting Information section.

2.4. Tests of the Anti-Fouling Ability of Membranes

A circular diaphragm with a diameter of 3.2 cm was cut, moistened with ultrapure water, and fixed in an ultrafilter cup (MSC50). The pure water flux (J) of the membranes was measured at 0.1 MPa using Equation (1) [35]. Then, 0.1 g/L of the bovine serum albumin (BSA) solution was filtered through the membrane. After 30 min of filtration, the water flux of the contaminated membrane was tested using ultrapure water. The flux attenuation coefficient is calculated as Equation (2) [36]:

$$J = \frac{V}{S \times t} \quad (1)$$

where J (L/m²·h) is the pure water flux at 0.1 MPa, V (L) is the volume of water penetrating the membrane in time t , S (m²) is the membrane area penetrated by water, and t (h) is the measured time.

$$m = \frac{J_0 - J_1}{J_0} \quad (2)$$

where J_0 and J_1 represent the pure water flux of the membrane before and after filtration with a BSA solution, respectively. A smaller m value indicates a stronger anti-fouling property of the membrane.

3. Results

3.1. Characterization

3.1.1. Morphology

Figure 1(a1–a4) were referenced from our previous research [29]. In the non-solvent-phase transformation process, the formation of a dense top layer directly affected the development of the supporting sub-layer with a porous structure. In the absence of PVP and VT, an instantaneous liquid–liquid split phase occurred on the membrane surface, resulting in the formation of a macroporous structure owing to the low viscosity of the casting solution (Figure 1(a1)). These surface macropores facilitated the exchange between the solvent in the casting solution and the non-solvent in the coagulation bath. In particular, the solvent in the sub-layer diffused outward into the coagulation bath at a higher rate than the non-solvent diffused into the membrane. Consequently, the liquid membrane shrank, resulting in a thinner top layer and the formation of finger-like holes in the internal

structure (Figure 1(a2–a4)). After introducing PVP and VT-M into the casting solution, the viscosity of the casting solution increased, leading to a delayed liquid–liquid phase separation. This resulted in an increased thickness and reduced pore diameter of the top layer (Figure 1(b1)), which hindered the solvent outflow from the supporting sub-layer. Moreover, the sub-layer exhibited a reduced pore diameter and an increased thickness owing to the lower rate of liquid membrane shrinkage (Figure 1(b2,b4)). Additionally, the membrane structure comprised numerous crosslinking PVP gel particles (Figure 1(b3)), which contributed to the improved hydrophilicity and effectively prevented the loss of PVP, thereby enhancing the hydrophilic stability. Figure 2 shows the photographs of the mixed-matrix PVDF membrane before and after drying.

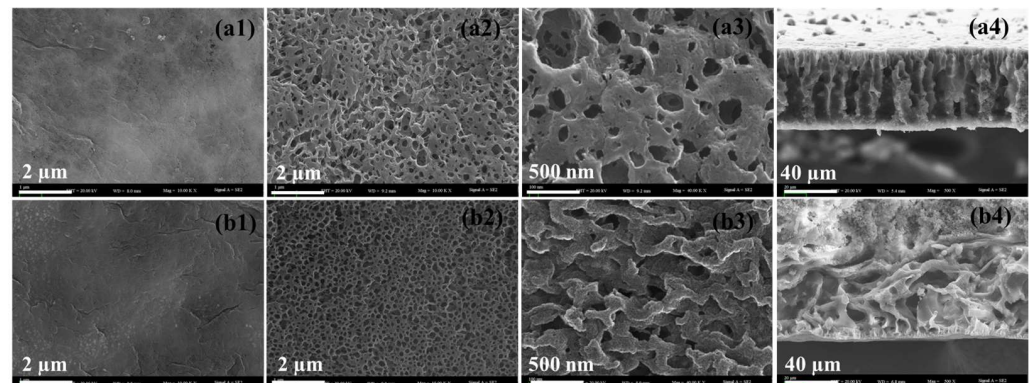


Figure 1. Morphologies of the top layer surfaces (a1,b1), sub-layer surfaces (a2,b2), magnified sub-layer surfaces (a3,b3), and cross-sections (a4,b4) of PVDF-based membranes. Scanning electron microscopy (SEM) images of (a) PEI-modified PVDF and (b) mixed-matrix PVDF membrane.

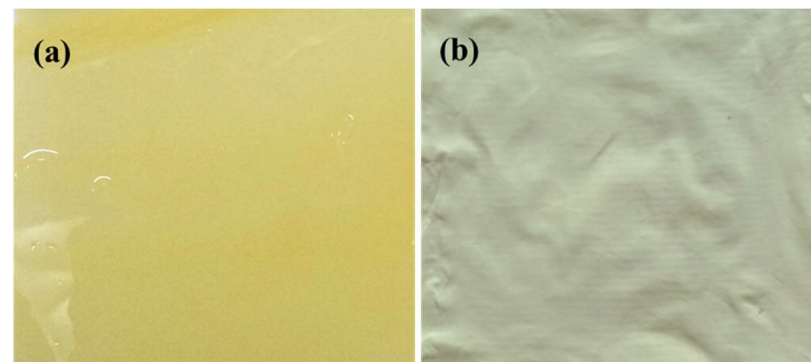


Figure 2. Photographs of the mixed-matrix PVDF membrane before drying (a) and after drying (b).

3.1.2. Membrane Hydrophilicity and Mechanical Strength

Generally, a smaller static water contact angle indicates higher surface hydrophilicity, a faster dynamic contact angle change, and greater material wettability [37]. In the first 1 s, the mixed-matrix PVDF membrane featured a static water contact angle of 34.4° (Figure 3b), which is significantly smaller than that of the PVDF/PEI membrane at 100.6° (Figure 3a). Figure 3c shows the dynamic contact angle curves of the samples. Notably, after 11 s of drop aging, the contact angle of the PVDF/PEI membrane did not decrease, indicating its water stability. In contrast, the water contact angle of the mixed-matrix PVDF membrane decreased to 0° after 7 s. This significant change was attributable to the introduction of hydrophilic PVP into the membrane matrix. A comparison of the pollution resistance between the PVDF/PEI membrane and the mixed-matrix PVDF membrane is shown in Table S1, with their m values being 0.96 and 0.11, respectively. A smaller m value indicates a stronger anti-fouling property, suggesting that the mixed-matrix PVDF membrane exhibited significantly higher excellent anti-fouling ability. Pure water fluxes of the PVDF/PEI

membrane and the mixed-matrix membrane after different numbers of immersion and drying processes are shown in Figure S1. The hydrophilic stability of the mixed-matrix PVDF membrane was better than that of the PVDF/PEI membrane. At the beginning of the experiment, some uncrosslinked PVP still existed in the membrane, and the water flux was large. With the increase in the water permeation times, the uncrosslinked PVP dissolved gradually from the membrane into the water, and the crosslinked PVP remained in the membrane, maintaining the hydrophilicity of the membrane and leading to the stable water flux of the mixed-matrix PVDF membrane.

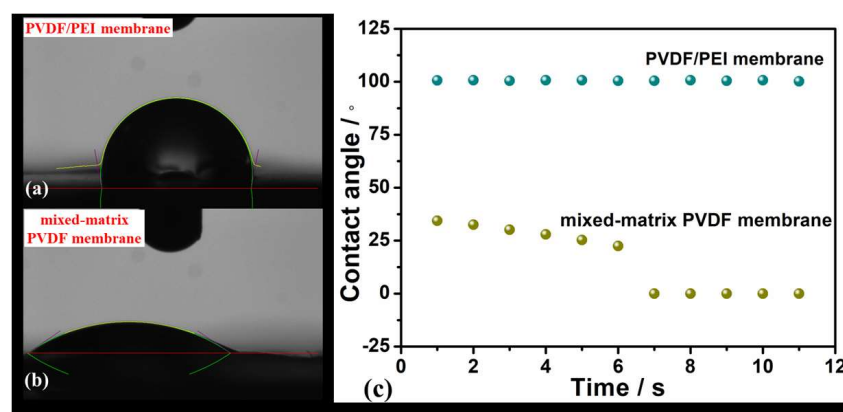


Figure 3. Static contact angles of the original membrane (a) and the modified membrane (b); dynamic contact angle curves of the original and modified membranes (c).

As an adsorbent, the mixed-matrix PVDF membrane requires a certain level of mechanical strength, particularly tensile strength, to reduce the risk of membrane breakage during adsorption and solid–liquid separation processes. Therefore, the mechanical strength of the as-prepared membranes was measured using a universal machine. The mixed-matrix PVDF membrane modified by VT-M exhibited a maximum tensile stress of 2.093 Mpa, which increased by 2.5 times that of the PVDF/PEI/PVP membrane (Figure 4). An interaction existed between VT-M nanoparticles and the polymer matrix. VT-M served as a crosslinking point in the composite membrane to connect the polymer chain (similar to reinforced concrete) and enhance the rigidity of the polymer chain. When a tensile stress was applied to the polymer chain, the binding force was able to be transferred laterally to the other polymer chain through the crosslinking point, at which point the impact energy was dispersed and the mechanical strength was maintained. Therefore, breaking the bond between VT-M and the polymer matrix required additional energy. Consequently, this led to increased tensile strength and improved mechanical properties of the membrane.

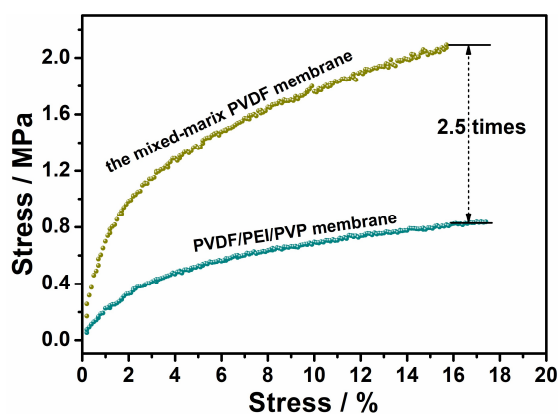


Figure 4. Tensile stress curves of the membranes; the measuring parameters were fixed: membranes with a thickness of 100 μm , a width of 1 cm, and a length of 10 cm; tensile speed: 20 mm/min.

3.2. Adsorption Studies

3.2.1. Effects of Contact Time and Solution pH on Adsorption

The conditions were maintained at a constant initial concentration of 400 mg/L, 20 mg of adsorbent per 20 mL, an adsorption temperature of 30 °C, and an adsorption time of 720 min. Figure 5a shows the analysis of the adsorption efficiency of the adsorbent on Hg(II) ions over time. In the first 60 min, the adsorption amount of Hg(II) ions significantly increased, reaching an adsorption rate of over 90%, and then the rate decreased. Consequently, the equilibrium was reached after 720 min, and the adsorbent featured an experimental equilibrium adsorption capacity of 396.4 mg/g. The solution acidity featured a certain effect on the adsorption capacity of the complex (Figure 5b). The adsorption rate of Hg(II) ions decreased with decreasing pH levels. As the pH level decreased from 5.5 to 1.5, the removal rate of Hg(II) ions decreased from 99.1% to 85.5%. This decrease was attributable to the protonation of the active functional group at low pH, resulting in higher positive charges on the adsorbent surface. During this time, excess protons in the aqueous solution with a low pH competed with Hg(II) ions and occupied the active sites. However, as the initial pH increased, the active functional group gradually lost protons, and the competitive effect of protons weakened, thereby improving the adsorption efficiency of Hg(II) ions. Figure S2 shows the zeta potentials of the mixed-matrix membrane as a function of pH, and the pH at the zero potential point is 7.32. The adsorption efficiency (E), however, still exceeded 85% at a pH of 1.5, indicating the superior acid resistance of the membrane. Moreover, the adsorption involved is a synergistic effect of chemical chelation and electrostatic attraction rather than a single effect. To prevent interference due to the precipitation of the Hg(II) ions and its effect on the adsorption capacity, pH 5.5 was selected for the follow-up study.

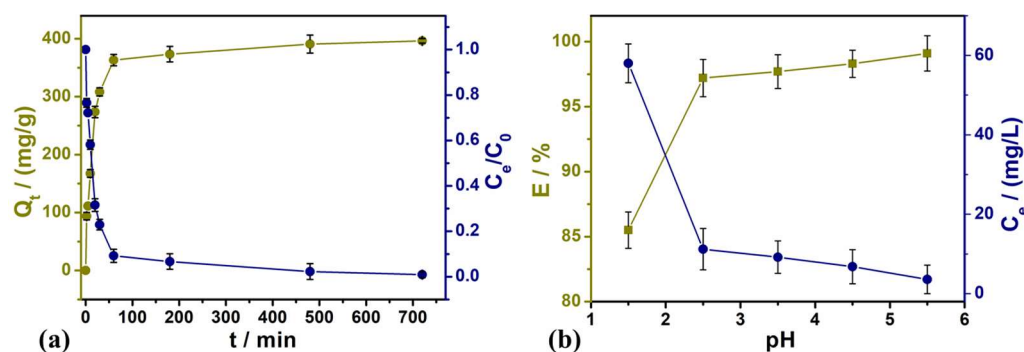


Figure 5. Dependence of the adsorption capacity on contact time (a); effect of solution pH on Hg(II) ion adsorption by the mixed-matrix membrane (b). (Except for the investigated parameters, others were fixed at $C_0 = 400.0$ mg/L, sample dosage = 20 mg/20 mL, temperature = 30 °C, pH = 5.5, and adsorption time = 720 min).

3.2.2. Effects of Co-Existing Ions and Reusability

In a single metal ion solution (Figure 6a), the mixed-matrix membrane exhibited a loading capacity of 396.4 mg/g for Hg(II) ions, which is significantly higher than that of other metal ions. The decreasing order of adsorption capacity among various metal ions was Hg(II) > Pb(II) > Cu(II) > Cd(II). Among the four common heavy metal ion mixed solutions, the composite membrane exhibited adsorption capacities of 273.5, 46.3, 47.3, and 0.007 mg/g for Hg(II), Pb(II), Cu(II), and Cd(II) ions, respectively (Figure 6b). This indicates that the membrane effectively removed Hg(II) ions and featured a certain removal capacity for Pb(II) and Cu(II) ions. However, the membrane could not adsorb Cd(II) ions, and the selectivity of the membrane for Hg(II) ions was 1.2×10^5 times that for Cd(II) ions (Table 1). This property made the membrane suitable for the efficient and selective removal of Hg(II) ions from wastewater containing Cd(II). Additionally, common anions (Cl^- , NO_3^- , SO_4^{2-} , H_2PO_4^- , and CH_3COO^-) were selected as co-existing anions to investigate their effect

on the adsorption capacity of the adsorbent, with Na⁺ as the cation. The result is shown in Figure 6c. NO₃⁻ and CH₃COO⁻ featured no significant effect on the adsorption rate of the membrane. However, Cl⁻, SO₄²⁻, and H₂PO₄⁻ led to a significant decrease in the adsorption rate, with a maximum decrease of 20%. The mixed-matrix PVDF composite membrane loaded with the Hg(II) ions can be desorbed using a 2 mol/L HCl solution and then regenerated using a dilute NaOH solution successively. After five sorption–desorption cycles, the adsorption rate of the membrane remained above 90% (Figure 6d). The SEM mapping images of the mixed-matrix membrane after the adsorption of single and mixed-metal ions are shown in Figures 7 and 8, respectively.

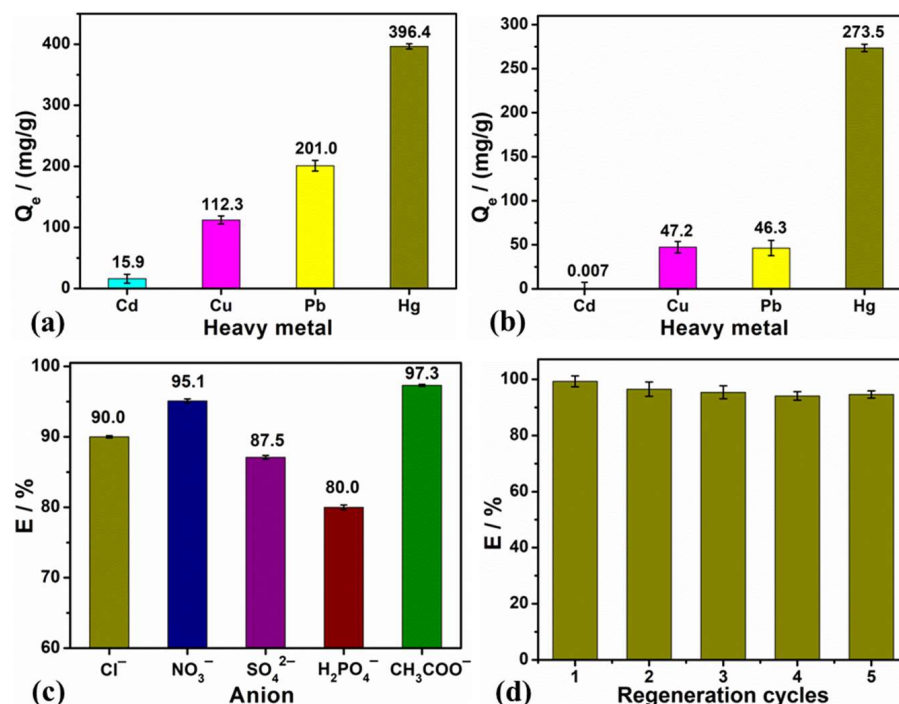


Figure 6. Adsorption result of the single metal ion solution (a); adsorption result of the mixed-metal ion solution (b); interference effect of anions (c) (concentration of anion: 50 mmol/L), reusability test on the adsorption capacity of the mixed-matrix membrane for Hg(II) ions (d). (Except for the investigated parameters, others were fixed at $C_0 = 400.0$ mg/L, sample dosage = 20 mg/20 mL, temperature = 30 °C, pH = 5.5, and adsorption time = 720 min.)

Table 1. Selectivity of the mixed-matrix membrane to Hg(II) ions in multi-component solution.

Ions	C_0 (mg/L)	C_e (mg/L)	Q_e (mg/g)	E (%)	K_d (mL/g)	$K_{\text{Hg/Cd}}$	$K_{\text{Hg/Cu}}$	$K_{\text{Hg/Pb}}$
Hg(II)	400.0	126.5	273.5	68.4%	2.16	1.2×10^5	16.6	16.6
Cd(II)	400.0	399.993	0.007	0.002%	1.8×10^{-5}			
Cu(II)	400.0	352.8	47.2	11.8%	0.13			
Pb(II)	400.0	353.7	46.3	11.6%	0.13			

3.3. Adsorption Mechanism

Pseudo-first-order [38], pseudo-second-order [39], and intraparticle diffusion models [40] were used to fit the test results. The results are shown in Figure 9a,b and Table 2. The adsorption of Hg(II) ions by the mixed-matrix membrane was best fitted with the pseudo-second-order kinetic model ($R^2 = 0.9997$), and the fitted equilibrium adsorption capacity predicted by this model was 400.0 mg/g, consistent with the experimental result. This indicates that the adsorption process was controlled by the chemisorption mechanism, which involves electron sharing or electron transfer between the adsorbent and the Hg(II) ions. This was mainly due to the chelation of Hg(II) ions with the coordination atoms of the

active functional groups on the membrane. The adsorption process comprised two steps. In the first step, Hg(II) ions gradually moved from the solution to the surface of the membrane and diffused into its interior structure. This phase lasted for ~60 min and can be classified as the rapid absorption phase. In the second step, the adsorption rate decreased, and the adsorption approached equilibrium owing to the low concentration of the remaining Hg(II) ions in the solution. Therefore, the removal of Hg(II) ions by the membrane involved physicochemical processes occurring at the adsorbent–solution interface (such as dissolution, chelation, ion exchange, and electrostatic attraction) and the diffusion process of Hg(II) ions. The adsorption isotherm of Hg(II) ions on the mixed-matrix membrane is shown in Figure 9c. With the increasing initial concentration of Hg(II) ions, the adsorption capacity of the membrane correspondingly increased, eventually reaching saturation ($Q_e = 771$ mg/g). Even in a wide range of initial concentrations (0.05–1000 mg/L), the removal efficiency of Hg(II) ions remained above 90%. To further elucidate the adsorption mechanism, Langmuir and Freundlich models [41–43] were used to fit the experimental data, and the results are shown in Table 3. The Langmuir model ($R^2 = 0.9620$) featured a higher degree of fitting than the Freundlich model ($R^2 = 0.8892$) and yielded a fitted Q_m value of 807 mg/g. This indicates that the adsorption process involved monolayer adsorption with both adsorption sites and adsorption energy [44–46].

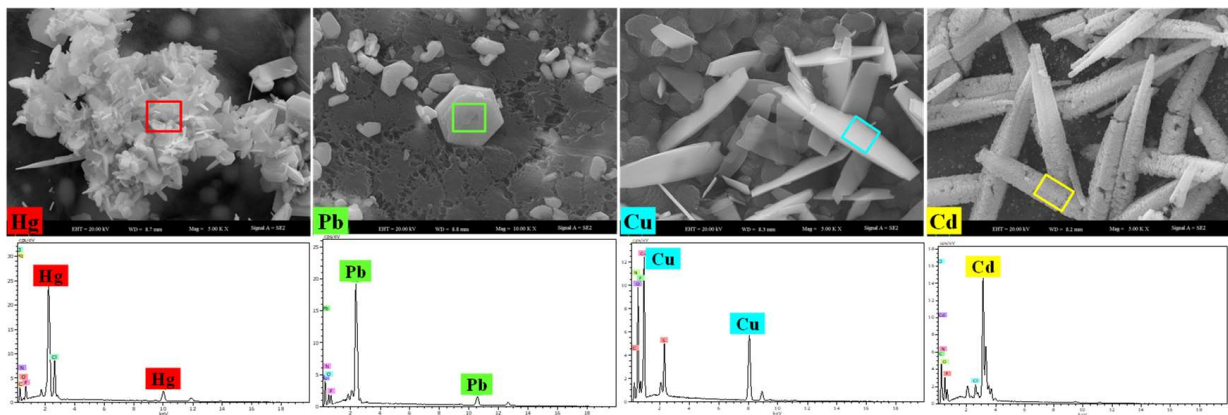


Figure 7. SEM mapping images of the mixed-matrix PVDF membrane after adsorption of single metal ions.

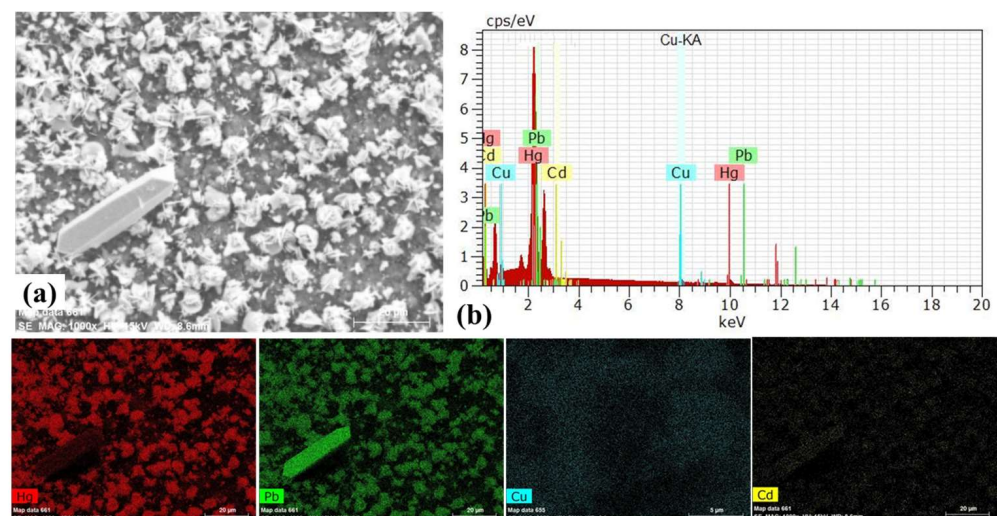


Figure 8. SEM mapping images (a) and EDS (b) of the mixed-matrix PVDF membrane after adsorption of mixed metal ions.

X-ray photoelectron spectroscopy (XPS) was used to further analyze the adsorption mechanism (Figure 10). Compared with the sample before adsorption, the XPS spectrum of the sample after adsorption featured significant signals of Hg (Hg 4f, Hg 4d, and Hg 4p, Figure 10), confirming the successful loading of Hg(II) on the membrane. Figure 10b, c, and d show the high-resolution spectra of C 1s, N 1s, and O 1s, respectively. After adsorption, the binding energy peak of C 1s at 286.1 eV shifted to 286.3 eV, indicating the formation of C=N, possibly due to the partial oxidation of amino groups. Additionally, the binding energy position of N 1s changed, with the two peaks at 397.8 and 399.1 eV shifting to 398.7 and 399.7 eV, respectively, accompanied by a significant decrease in peak intensity. This result confirmed the strong chelation between N and Hg. After coordination between N and Hg, the electron cloud density of N atoms decreased, resulting in a higher binding energy. Furthermore, the O 1s spectrum featured a change, with peaks at 529.5 and 530.4 eV combining into one peak at 530.5 eV. This indicates that the surface O of the composite membrane was involved in the adsorption process of Hg(II) ions. The analysis results of kinetics, isothermal adsorption, SEM, and XPS revealed that the adsorption of the Hg(II) ion by the mixed-matrix membrane was a comprehensive process involving both chemical and physical adsorption, including diffusion, chemical chelation, electrostatic attraction, and crystal growth.

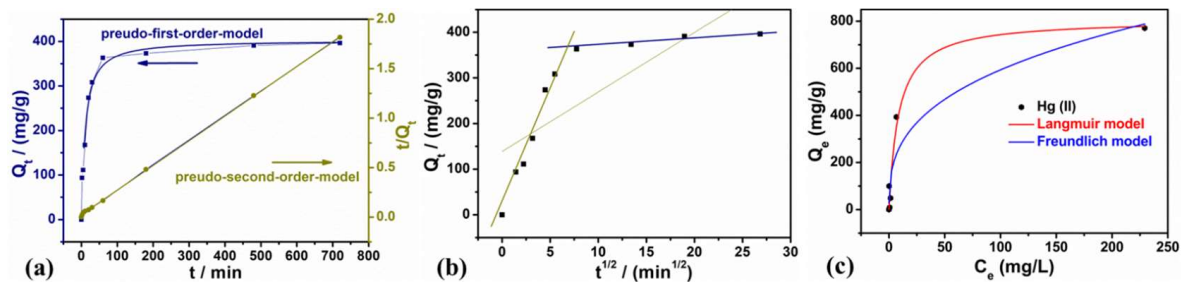


Figure 9. Fitting results for pseudo-first-order model and pseudo-second-order model (a); intraparticle diffusion model (b); adsorption isotherms of Hg(II) ions on the modified membrane (c). (Except for the investigated parameters, others were fixed at $C_0 = 400.0$ mg/L, sample dosage = 20 mg/20 mL, temperature = 30 °C, pH = 5.5, and adsorption time = 720 min.)

Table 2. Kinetic parameters for the adsorption of Hg(II) onto the modified membrane.

Q_f (mg/g)	Pseudo-First-Order Model	R^2
402.0	k_1 (1/min) 0.0283	0.9701
Q_f (mg/g)	Pseudo-second-order model	R^2
400.0	k_2 [g/(mg·min)] 2.8×10^{-4}	0.9997
θ	Intraparticle diffusion model	R^2
138.5	k_{int} [mg/(g·min ^{1/2})] 13.04	0.3540

Table 3. Fitted parameters of the adsorption isotherms.

Q_m (mg/g)	Langmuir Model	R^2
807	b_L (L/mg) 0.12	0.9620
K_F	Freundlich model	R^2
113	n_F 0.34	0.8892

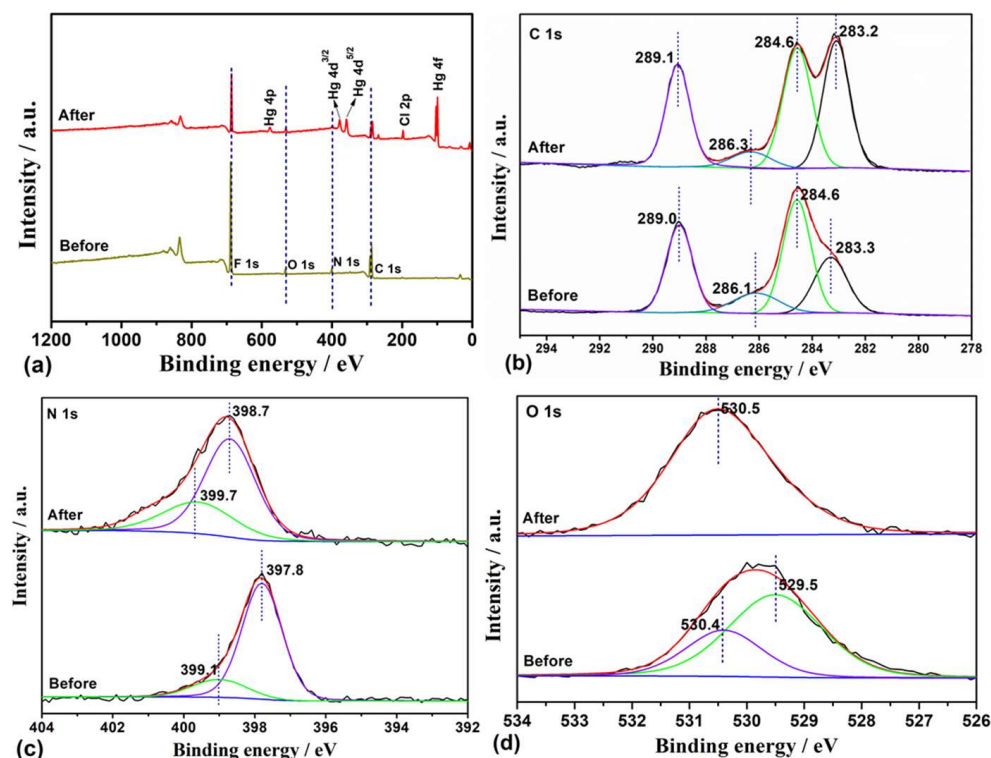


Figure 10. (a) XPS spectra of the survey; (b) C 1s; (c) N 1s; (d) O 1s of the mixed-matrix membrane before and after Hg(II) ion adsorption.

4. Conclusions

A modified mixed-matrix membrane was successfully prepared for removing Hg(II) ions from water. Owing to its numerous active functional groups, the membrane exhibited excellent Hg(II) ion adsorption capacity, with a maximum fitted adsorption capacity of 807 mg/g. The adsorption mechanism of the Hg(II) ions involved the single-molecular-layer adsorption of uniform active sites. Additionally, the introduction of PVP and VT-M considerably improved the hydrophilic ability of the composite film and enhanced its tensile resistance. Therefore, the mixed-matrix membrane adsorbent is considered an ideal material for removing heavy metal ions from contaminated water.

Supplementary Materials: The following supporting information can be downloaded at: <https://www.mdpi.com/article/10.3390/pr12010030/s1>, Figure S1: Pure water flux of PVDF/PEI membrane and mixed-matrix membrane after different number of times of the immersion and drying occurred; Figure S2: Relationship between Zeta potential of the mixed-matrix membrane and pH; Table S1: The results of pollution resistance tests.

Author Contributions: C.W. and H.Z. conceived and designed the experiments; L.C. and X.W. performed the experiments; W.H., J.L. and G.Z. analyzed the data; F.H. and X.M. contributed reagents/materials/analysis tools; L.C. wrote the paper. All authors have read and agreed to the published version of the manuscript.

Funding: This research received no external funding.

Data Availability Statement: The data are available upon request.

Acknowledgments: This study was financially supported by the National Nature Science Foundation of China (Grant Nos. 52000011 and 52260008) and the Natural Science Foundation of Xin-jiang Uygur Autonomous Region (2022D01C464). We thank LetPub (www.letpub.com, URL (accessed on 8 December 2023)) for its linguistic assistance during the preparation of this manuscript.

Conflicts of Interest: The authors declare no conflict of interest.

Lists of Symbols and Acronyms

Hg	Mercury
PVDF	Polyvinylidene fluoride
PEI	Polyethyleneimine
PVP	Polyvinylpyrrolidone
VT	Vermiculite
Q_e (mg/g)	Adsorption capacity
E	Adsorption efficiency
C_0 and C_e	Initial and equilibrium concentrations (mg/L)
V (L)	Volume of the solution
m (g)	Mass of the adsorbent
K_d	The distribution coefficient
Q_m	Theoretical maximum adsorption capacity (mg/g)
C_e	Final equilibrium mercury concentration (mg/L)
b_L	Langmuir constant (L/mg) related to the adsorption strength
K_F	Freundlich constant related to the adsorption strength (mg/g) (L/mg)
n_F	Freundlich constant related to the adsorption capacity

References

- Zhou, Y.C.; Ma, S.; Zhu, W.H.; Shi, Q.Q.; Jiang, H.Q.; Lu, R.; Wu, W.J. Revealing varying relationships between wastewater mercury emissions and economic growth in Chinese cities. *Environ. Pollut.* **2023**, *341*, 122944. [[CrossRef](#)] [[PubMed](#)]
- Li, J.S.; Song, X.H.; Guo, Y.Q.; Yang, Q.; Feng, K.S. The determinants of China's national and regional energy-related mercury emission changes. *J. Environ. Manag.* **2019**, *246*, 505–513. [[CrossRef](#)] [[PubMed](#)]
- Chen, B.; Li, J.S.; Chen, G.Q.; Wei, W.D.; Yang, Q.; Yao, M.T.; Shao, J.A.; Zhou, M.; Xia, X.H.; Dong, K.Q.; et al. China's energy-related mercury emissions: Characteristics, impact of trade and mitigation policies. *J. Clean. Prod.* **2017**, *141*, 1259–1266. [[CrossRef](#)]
- Liu, C.; Peng, J.H.; Liu, J.; Guo, P.; Wang, S.X.; Liu, C.H.; Zhang, L.B. Catalytic removal of mercury from waste carbonaceous catalyst by microwave heating. *J. Hazard Mater.* **2018**, *358*, 198–206. [[CrossRef](#)]
- Li, W.X.; Ju, B.Z.; Zhang, S.F. Preparation of cysteamine-modified cellulose nanocrystal adsorbent for removal of mercury ions from aqueous solutions. *Cellulose* **2019**, *26*, 4971–4985. [[CrossRef](#)]
- Liu, Y.Y.; Chen, Y.; Li, Y.R.; Li, Y.Q.; He, C.Y. Thioether-functionalized covalent organic framework for mercury removal. *Colloid Surface A* **2024**, *681*, 132807. [[CrossRef](#)]
- Tami-Pimiento, L.M.; Joya-Herrera, L.M.; Pérez-Chía, Y.I.; Meléndez, A.M. Selective electrochemical reduction of mercury(II) from a simulated traditional gold mining wastewater contaminated with cyanide and heavy metals. *J. Solid State Electrochem.* **2023**, *363*, 192–202. [[CrossRef](#)]
- Agostino, F.; Bellante, A.; Bonsignore, M.; Core, M.D.; Clarizia, L.; Sabatino, N.; Giaramita, L.; Tranchida, G.; Chiavarini, S.; Sprovieri, M. A chemical remediation technique for a nearly-total removal of arsenic and mercury from contaminated marine sediments. *Heliyon* **2023**, *9*, e22633. [[CrossRef](#)]
- Bessbousse, H.; Rhallou, T.; Verchère, J.F.; Lebrun, L. Sorption and filtration of Hg(II) ions from aqueous solutions with a membrane containing poly(ethyleneimine) as a complexing polymer. *J. Membr. Sci.* **2008**, *325*, 997–1005. [[CrossRef](#)]
- Zhang, L.P.; Liu, Z.; Zhou, X.L.; Zhang, C.; Cai, Q.W.; Xie, R.; Ju, X.J.; Wang, W.; Faraj, Y.; Chu, L.Y. Novel composite membranes for simultaneous catalytic degradation of organic contaminants and adsorption of heavy metal ions. *Sep. Purif. Technol.* **2020**, *237*, 116364. [[CrossRef](#)]
- Zia, Q.; Tabassum, M.; Meng, J.M.; Xin, Z.Y.; Gong, H.; Li, J.S. Polydopamine-assisted grafting of chitosan on porous poly (L-lactic acid) electrospun membranes for adsorption of heavy metal ions. *Int. J. Biol. Macromol.* **2021**, *167*, 1479–1490. [[CrossRef](#)] [[PubMed](#)]
- Zhu, F.; Zheng, Y.M.; Zhang, B.G.; Dai, Y.R. A critical review on the electrospun nanofibrous membranes for the adsorption of heavy metals in water treatment. *J. Hazard Mater.* **2021**, *401*, 123608. [[CrossRef](#)] [[PubMed](#)]
- Zhao, X.H.; Li, J.; Mu, S.Y.; He, W.; Zhang, D.; Wu, X.; Wan, C.Y.; Zeng, H.H. Efficient removal of mercury ions with MoS₂-nanosheet-decorated PVDF composite adsorption membrane. *Environ. Pollut.* **2021**, *268*, 115705. [[CrossRef](#)] [[PubMed](#)]
- Pariy, I.O.; Ivanova, A.A.; Shvartsman, V.V.; Lupascu, D.C.; Sukhorukov, G.B.; Surmeneva, M.A.; Surmenev, R.A. Poling and annealing of piezoelectric poly(vinylidene fluoride) micropillar arrays. *Mater. Chem. Phys.* **2020**, *239*, 122035. [[CrossRef](#)]
- Pariy, I.O.; Ivanova, A.A.; Shvartsman, V.V.; Lupascu, D.C.; Sukhorukov, G.B.; Ludwig, T.; Bartasyte, A.; Mathur, S.; Surmeneva, M.A.; Surmenev, R.A. Piezoelectric response in hybrid micropillar arrays of poly(vinylidene fluoride) and reduced graphene oxide. *Polymers* **2019**, *11*, 1065. [[CrossRef](#)] [[PubMed](#)]

16. He, S.J.; Zhai, S.X.; Zhang, C.; Xue, Y.; Yang, W.; Lin, J. Effect of sulfonation degree and PVDF content on the structure and transport properties of SPEEK/PVDF blend membranes. *Polymers* **2019**, *11*, 276. [[CrossRef](#)] [[PubMed](#)]
17. Li, C.C.; Chen, X.Y.; Luo, J.; Wang, F.; Liu, G.J.; Zhu, H.L.; Guo, Y.H. PVDF grafted Gallic acid to enhance the hydrophilicity and antibacterial properties of PVDF composite membrane. *Sep. Purif. Technol.* **2021**, *259*, 118127. [[CrossRef](#)]
18. Munirasu, S.; Banat, F.; Durrani, A.A.; Haija, M.A. Intrinsically superhydrophobic PVDF membrane by phase inversion for membrane distillation. *Desalination* **2017**, *417*, 77–86. [[CrossRef](#)]
19. Javadi, M.; Jafarzadeh, Y.; Yegani, R.; Kazemi, S. PVDF membranes embedded with PVP functionalized nanodiamond for pharmaceutical wastewater treatment. *Chem. Eng. Res. Des.* **2018**, *140*, 241–250. [[CrossRef](#)]
20. Li, J.; Sun, J.; Ren, L.; Lei, T.; Li, J.; Jin, J.; Luo, S.; Qin, S.; Gao, C.; Lei, T. Properties and preparation of TiO₂-HAP@PVDF composite ultrafiltration membranes. *Polym. Compos.* **2023**, *44*, 7499–7509. [[CrossRef](#)]
21. Zhao, Y.H.; Zhu, B.K.; Kong, L.; Xu, Y.Y. Improving hydrophilicity and protein resistance of poly(vinylidene fluoride) membranes by blending with amphiphilic hyperbranched-star polymer. *Langmuir* **2007**, *23*, 5779–5786. [[CrossRef](#)] [[PubMed](#)]
22. Liu, J.; Shen, X.; Zhao, Y.; Chen, L. Acryloylmorpholine-grafted PVDF membrane with improved protein fouling resistance. *Ind. Eng. Chem. Res.* **2013**, *52*, 18392–18400. [[CrossRef](#)]
23. Ning, L.; Yu, T.; Zhang, J.; Sun, Z.; Zhao, J.; Jian, Z.; Wei, Z. Precisely-controlled modification of PVDF membranes with 3D TiO₂/ZnO nanolayer: Enhanced anti-fouling performance by changing hydrophilicity and photocatalysis under visible light irradiation. *J. Membrane Sci.* **2017**, *528*, 359–368.
24. Xiang, S.; Xie, T.; Wang, J.; Fan, W. Improved fouling resistance of poly(vinylidene fluoride) membrane modified with poly(acryloyl morpholine)-based amphiphilic copolymer. *Colloid Polym. Sci.* **2017**, *295*, 1211–1221.
25. Zhang, S.; Shen, J.; Qiu, X.; Weng, D.; Zhu, W. ESR and vibrational spectroscopy study on poly(vinylidene fluoride) membranes with alkaline treatment. *J. Power Sources* **2006**, *153*, 234–238. [[CrossRef](#)]
26. Guo, G.B.; Kou, S.S.; An, S.L. Effect factors of the stem grafting rate of the PVDF-g-PSSA membrane modified by the plain sodium silicate (Na₄SiO₄). *Polym. Mater. Eng.* **2010**, *26*, 93–96.
27. Estrada-Villegas, G.M.; Bucio, E. Comparative study of grafting a polyampholyte in a fluoropolymer membrane by gamma radiation in one or two-steps. *Radiat. Phys. Chem.* **2013**, *92*, 61–65. [[CrossRef](#)]
28. Dong, L.; Liu, X.D.; Xiong, Z.R.; Sheng, D.K.; Lin, C.H.; Zhou, Y.; Yang, Y. Preparation and characterization of functional poly(vinylidene fluoride) (PVDF) membranes with ultraviolet-absorbing property. *Appl. Surf. Sci.* **2018**, *444*, 497–504. [[CrossRef](#)]
29. Zeng, H.H.; Wang, L.; Zhang, D.; Wang, C.Y. Efficient capture and detoxification of mercury dichloride from wastewater by a PVDF/PEI adsorption membrane. *Chem. Eng. J.* **2023**, *468*, 143621. [[CrossRef](#)]
30. Ike, I.A.; Dumée, L.F.; Groth, A.; Orbell, J.D.; Duke, M. Effects of dope sonication and hydrophilic polymer addition on the properties of low pressure PVDF mixed matrix membranes. *J. Membr. Sci.* **2017**, *540*, 200–211. [[CrossRef](#)]
31. Guo, H.H.; Yang, J.; Zhao, W.Q.; Xu, T.; Lin, C.G.; Zhang, J.W.; Zhang, L. Direct formation of amphiphilic crosslinked networks based on PVP as a marine anti-biofouling coating. *Chem. Eng. J.* **2019**, *374*, 1353–1363. [[CrossRef](#)]
32. Leone, G.; Consumi, M.; Lamponi, S.; Bonechi, C.; Tamasi, G.; Donati, A.; Rossi, C.; Magnani, A. Thixotropic PVA hydrogel enclosing a hydrophilic PVP core as nucleus pulposus substitute. *Mat. Sci. Eng.-C* **2019**, *98*, 696–704. [[CrossRef](#)] [[PubMed](#)]
33. Wardani, A.K.; Ariono, D.; Subagio, S.; Wenten, I.G. Fouling tendency of PDA/PVP surface modified PP membrane. *Surf. Interfaces* **2020**, *19*, 100464. [[CrossRef](#)]
34. Gu, S.Q.; Wang, L.; Mao, X.Y.; Yang, L.P.; Wang, C.Y. Selective adsorption of Pb(II) from aqueous solution by triethylenetetramine-grafted polyacrylamide/vermiculite. *Materials* **2018**, *11*, 514. [[CrossRef](#)] [[PubMed](#)]
35. Ji, J.; Zhou, S.Y.; Lai, C.Y.; Wang, B.; Li, K. PVDF/palygorskite composite ultrafiltration membranes with enhanced abrasion resistance and flux. *J. Membr. Sci.* **2015**, *495*, 91–100. [[CrossRef](#)]
36. Wei, D.Y.; Zhou, S.Y.; Li, M.S.; Xue, A.L.; Zhang, Y.; Zhao, Y.J.; Zhong, J.; Yang, D.W. PVDF/palygorskite composite ultrafiltration membranes: Effects of nanoclay particles on membrane structure and properties. *Appl. Clay Sci.* **2019**, *181*, 105171. [[CrossRef](#)]
37. Wang, B.; Zhu, Y.; Bai, Z.; Luque, R.; Xuan, J. Functionalized chitosan biosorbents with ultra-high performance, mechanical strength and tunable selectivity for heavy metals in wastewater treatment. *Chem. Eng. J.* **2017**, *325*, 350–359. [[CrossRef](#)]
38. Azizian, S. Kinetic models of sorption: A theoretical analysis. *J. Colloid Interface Sci.* **2004**, *27*, 47–52. [[CrossRef](#)]
39. Ho, Y.S. Review of second-order models for adsorption systems. *J. Hazard. Mater.* **2006**, *136*, 681–689. [[CrossRef](#)]
40. Annadurai, G.; Juang, R.; Lee, D. Use of cellulose-based wastes for adsorption of dyes from aqueous solutions. *J. Hazard. Mater.* **2002**, *92*, 263–274. [[CrossRef](#)]
41. Tchinda, A.L.J.; Ngameni, E.; Kenfack, I.T.; Walcarius, A. One-step preparation of thiol-functionalized porous clay heterostructures: Application to Hg(II) binding and characterization of mass transport issues. *Chem. Mater.* **2009**, *21*, 4111–4121. [[CrossRef](#)]
42. Bessbousse, H.; Verchère, J.F.; Lebrun, L. Increase in permeate flux by porosity enhancement of a sorptive UF membrane designed for the removal of mercury(II). *J. Membr. Sci.* **2010**, *364*, 167–176. [[CrossRef](#)]
43. Gang, X.; Zhao, Y.; Hou, L.; Jian, C.; Tao, M.; Zhang, W. A recyclable phosphonic acid functionalized polyacrylonitrile fiber for selective and efficient removal of Hg²⁺. *Chem. Eng. J.* **2017**, *325*, 533–543.
44. Tang, H.; Chang, C.Y.; Zhang, L.N. Efficient adsorption of Hg²⁺ ions on chitin/cellulose composite membranes prepared via environmentally friendly pathway. *Chem. Eng. J.* **2011**, *173*, 689–697. [[CrossRef](#)]

45. Rabelo, R.B.; Vieira, R.S.; Luna, F.M.T.; Guibal, E.; Beppu, M.M. Adsorption of copper(II) and mercury(II) ions onto chemically-modified chitosan membranes: Equilibrium and kinetic properties. *Adsorpt. Sci. Technol.* **2012**, *30*, 1–21. [[CrossRef](#)]
46. Ballav, N.; Das, R.; Giri, S.; Muliwa, A.M.; Pillay, K. L-cysteine doped polypyrrole (PPy@L-Cyst): A super adsorbent for the rapid removal of Hg²⁺ and efficient catalytic activity of the spent adsorbent for reuse. *Chem. Eng. J.* **2018**, *345*, 621–630. [[CrossRef](#)]

Disclaimer/Publisher’s Note: The statements, opinions and data contained in all publications are solely those of the individual author(s) and contributor(s) and not of MDPI and/or the editor(s). MDPI and/or the editor(s) disclaim responsibility for any injury to people or property resulting from any ideas, methods, instructions or products referred to in the content.